Electronic band structure, transport, and magnetic properties of $Mo_{3-x}Ru_xSb_7$

C. Candolfi,* B. Lenoir, and A. Dauscher
Institut Jean Lamour, UMR 7198, CNRS–Nancy Université–UPVM, Ecole Nationale Supérieure des Mines de Nancy, Parc de Saurupt, 54042 Nancy Cedex, France

J. Hejtmánek
Institute of Physics, Academy of Sciences of the Czech Republic, Cukrovarnicka 10, CZ-162 53 Praha 6, Czech Republic

J. Tobola
Faculty of Physics and Applied Computer Science, AGH University of Science and Technology, 30-059 Krakow, Poland
(Received 20 July 2009; revised manuscript received 18 September 2009; published 20 October 2009)

Electrical and thermal transport properties, including thermopower, electrical resistivity, thermal conductivity, as well as Hall effect and magnetic susceptibility measurements have been carried out on polycrystalline $Mo_{3-x}Ru_xSb_7$ samples for nominal concentrations $x=0.0$, 0.25, 0.50, and 1.0 in the 2–350 K temperature range. Further insight into the variations in the electronic band structure as the Ru content increases has been gained by calculating dispersion curves and total and partial densities of states using the Korringa-Kohn-Rostoker method with the coherent-potential approximation. This theoretical analysis has revealed a rigidlike behavior of the electronic structure, synonymous of a shift in the Fermi level toward the valence band edge as x increases. Transport properties investigations have provided compelling experimental evidence for this picture, i.e., an increase in both the electrical resistivity and thermopower which is concomitant to a decrease in the charge-carrier concentration with x. Magnetic susceptibility data have shown that the magnetic interactions displayed by Mo_3Sb_7 are progressively suppressed by increasing the ruthenium concentration. In addition, increasing x leads to a surprising enhancement of the lattice thermal conductivity that may be due to the suppression of strong phonon-dimer interactions exhibited by Mo_3Sb_7.

DOI: 10.1103/PhysRevB.80.155127 PACS number(s): 72.20.Pa

I. INTRODUCTION

Among narrow-band-gap semiconductors and semimetals, intermetallic Zintl phases are currently focusing attention due to their promising thermoelectric properties.[1–6] Most of these materials can be considered to be valence precise, resulting in semiconducting properties that coupled with complex crystalline structures formed by heavy atoms in large unit cells constitute the prerequisites to achieve superior thermoelectric performance. The ability of a material to be a prospective candidate for thermoelectric applications can be quantitatively captured in the dimensionless figure of merit ZT defined as $ZT=\alpha^2T/\rho\lambda$, where α is the Seebeck coefficient or thermopower, ρ is the electrical resistivity, λ is the total thermal conductivity, and T is the absolute temperature.[7]

In an effort to search for new Zintl phases displaying higher thermoelectric efficiency, i.e., high ZT values, the $Yb_{14}MnSb_{11}$ compound was found to meet the above-mentioned qualifications leading to a maximum ZT of 1 at $\sim$1200 K.[8–11] Further optimization through judicious substitutions on both the rare earth and transition-metal sites have led to enhanced ZT values ($ZT\sim1.3$ at 1223 K in $Yb_{14}Mn_{1-x}Al_xSb_{11}$ for $x=0.6$ and 0.8) positioning these compounds as the best bulk p-type materials operating at these temperatures discovered up to now.[10]

Recently, other compounds qualified as Zintl phases and crystallizing in the M_3T_7 bcc structure have been investigated.[1,12–15] The crystallographic structure can be either described as a three-dimensional (3D) arrangement of antiprisms formed by the T atoms [Fig. 1(a)] or by considering how the M and T sublattices (bcc sublattice of octahedral structures and truncated octahedra, respectively) interpenetrate each other [Fig. 1(b)]. Among the various compounds discovered, both Mo_3Sb_7 and Re_3As_7 are the most intriguing materials not only for their thermoelectric properties but also from a fundamental point of view in the former case.[16–26] One of the essential features of these compounds lies in the existence of an energy gap separating the valence and conduction bands and arising from strong d-p orbitals hybridization.[12,14] Electronic band-structure investigations have shown that driving the system into a semiconducting regime of conduction could be realized through substitutions providing two electrons (Mo_3Sb_7) and one hole (Re_3As_7) per f.u., respectively.[12,14–16]

Of the various elements that could bring two additional electrons to the Mo_3Sb_7 electronic structure, Te proved to insert the crystalline lattice on the Sb site and to have a deep impact on the transport properties.[14,15,27,28] Upon substitution, a progressive increase in the electrical resistivity and thermopower is observed, consistent with a rigidlike behavior of the electronic structure suggested by theoretical calculations based on the Korringa-Kohn-Rostoker method including the coherent-potential approximation (KKR-CPA).[27] In addition, a disappearance of the magnetic interactions displayed by Mo_3Sb_7 that lead to the formation of a spin gap below $T^*=53$ K occurs when the Te content spans the range of $0\leq x\leq1.8$.[19,27] The thermal conduction processes are also drastically affected by this partial substitution, resulting in marked differences in the thermal conductivity temperature dependences as well as in an increase in the lattice thermal conductivity with x. This uncommon changeover from an

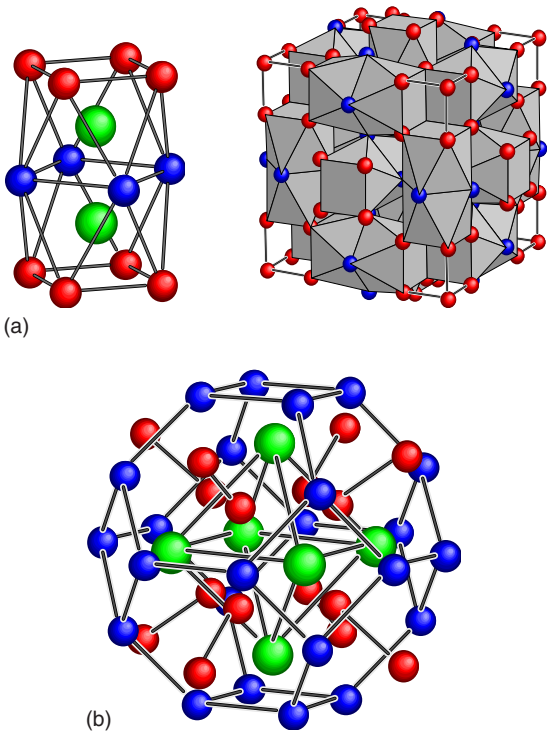

FIG. 1. (Color online) (a) (left picture) Elementary building blocks composed by two antiprisms formed by T atoms (in red and in blue, the different colors refer to the two distinct T sites that characterize this structure). The M atoms (in green) sit at the center of each antiprism. The crystal lattice is then formed by a 3D arrangement of the elementary blocks (right picture). (b) Alternatively, the crystal structure can be viewed as a 3D arrangement of truncated octahedra formed by the T atoms encapsulating a M octahedron.

exotic temperature dependence to a conventional behavior is concomitant with the progressive suppression of the magnetic interactions suggesting that molybdenum dimers act as efficient scattering centers in both Mo_3Sb_7 and $Mo_3Sb_{7-x}Te_x$ for low Te contents.[26,27] High Te concentrations strongly improve the thermoelectric properties of the Mo_3Sb_7 compound and lead to high ZT values that even surpass those of the best state-of-the-art thermoelectric materials, namely, Si-Ge alloys, operating in the 900–1200 K temperature range.[15,29]

Neutron diffraction experiments and low-temperature electrical resistivity measurements together with preliminary band-structure calculations have not only demonstrated that Mo can be partially substituted by Ru but they have also suggested a rigidlike behavior of the electronic structure with respect to the Ru content.[30] Even though a solubility limit ($x \sim 0.8$) of Ru that prevents the system being driven into a semiconducting state has been clearly demonstrated, high-temperature thermoelectric properties studies have revealed an enhancement of the ZT values for high Ru contents.[31]

Though optimum thermoelectric properties are achieved at high temperatures, to extend transport property measurements to liquid-helium temperature is required to shed light on the role of the Ru substitution in the microscopic mechanisms governing the thermal and electrical conduction processes. Moreover, since the antiferromagnetically coupled molybdenum dimers that characterize the Mo_3Sb_7 compound are directly affected by the insertion of Ru, this partial substitution may also provide valuable information regarding the influence of the low-dimensional magnetism on the transport properties of these materials. Thus, transport properties studies coupled with magnetic susceptibility measurements have been carried out on polycrystalline $Mo_{3-x}Ru_xSb_7$ samples with nominal composition $x=0$, 0.25, 0.50, and 1.0 in the 2–350 K temperature range. To further investigate the rigidlike behavior of the electronic structure, total site-decomposed and l-decomposed densities of states (DOS) have been calculated by the KKR-CPA method for all compositions. Dispersion curve calculations have also been undertaken on $x=0.25$ and 0.8 samples.

TABLE I. EPMA analysis, lattice parameter (a), and relative density (d) of the $Mo_{3-x}Ru_xSb_7$ compounds.

Nominal composition	EPMA	a (Å)	d (%)
Mo_3Sb_7	$Mo_3Sb_{6.95}$	9.568(8)	93%
$Mo_{2.75}Ru_{0.25}Sb_7$	$Mo_{2.75}Ru_{0.25}Sb_7$	9.550(4)	98%
$Mo_{2.5}Ru_{0.5}Sb_7$	$Mo_{2.5}Ru_{0.5}Sb_7$	9.524(9)	99%
Mo_2RuSb_7	$Mo_{2.2}Ru_{0.8}Sb_7$	9.500(8)	88%

II. EXPERIMENTAL AND COMPUTATIONAL DETAILS

Polycrystalline $Mo_{3-x}Ru_xSb_7$ samples with $x=0.0$, 0.25, 0.50, and 1.0 have been prepared by a solid-state reaction method. Stoichiometric quantities of high-purity Mo powders (99.999%), Sb powders (99.999%), and Ru powders (99.99%) were loaded into a quartz ampoule sealed under a reducing He-H_2 atmosphere. These ampoules were then heated in a vertical programmable furnace up to 750 °C for 10 days. The ingots were ground in an agate mortar into fine powders that were cold pressed and annealed under the same previous conditions for 15 days. The pellets were crushed, powdered and final densification was performed in graphite dies by hot pressing in an argon atmosphere at 600 °C for 2 h under 51 MPa. Structure and chemical composition were checked by x-ray diffraction, neutron diffraction, and electron probe microanalysis (EPMA).[30] As described in detail in previous investigations,[30] these experiments have unambiguously shown that the $x=0.0$, 0.25, and 0.50 samples are homogeneous with actual compositions close to nominal compositions. A small amount of $RuSb_2$ was detected in the $x=1.0$ sample indicative of a solubility limit of Ru in the Mo_3Sb_7 crystalline structure. The actual chemical compositions, the lattice parameters, and the relative densities of the different samples investigated are listed in Table I. In the next paragraphs the actual composition will always be used.

Thermoelectric properties including electrical resistivity, thermal conductivity, and thermopower were measured from 3.5 to 300 K by a steady-state method in an automated closed-cycle refrigerator system. Hall-effect measurements were carried out with an ac transport measurement system option of the physical properties measurement system

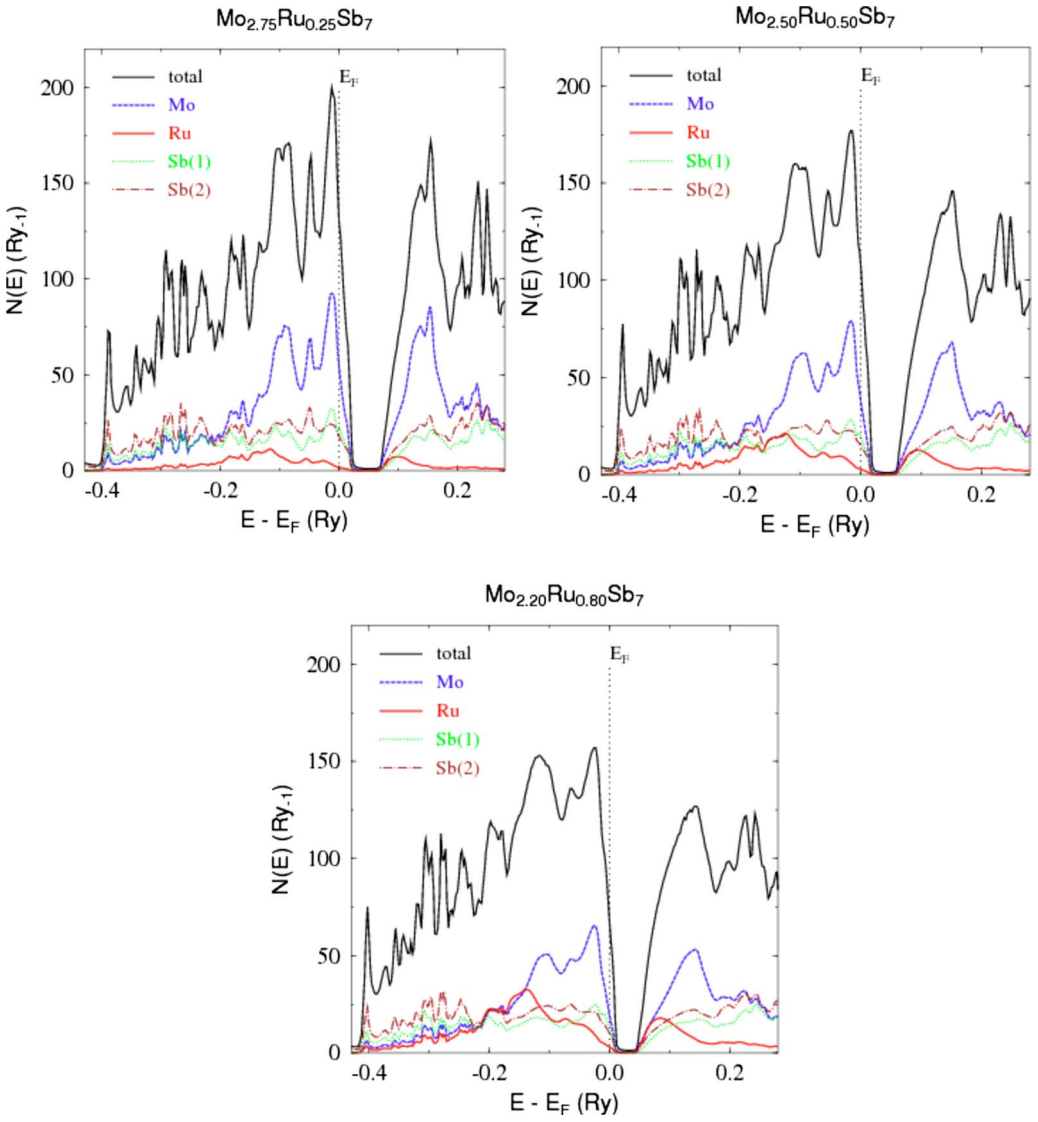

FIG. 2. (Color online) Energy dependence near the Fermi level of the total and site-decomposed DOS of the $x=0.25$, 0.5, and 0.8 samples.

(Quantum Design) over 5–300 K temperature range and under a magnetic field spanning the range from −7 to +7 T. Isothermal magnetization curves were measured from 5 to 300 K in applied fields of up to 7 T using a Quantum Design magnetometer (MPMS-Quantum Design).

Electronic band-structure calculations of $Mo_{3-x}Ru_xSb_7$ ($0.0 \leq x \leq 1.0$) were performed by the Korringa-Kohn-Rostoker method with the coherent-potential approximation to treat the chemical disorder on the Mo site.[32,33] The crystal potential of the *muffin-tin* form was constructed within the local-density approximation applying von Barth-Hedin formula for the exchange-correlation part. Dispersion curves with complex energies were calculated for the disordered alloys along high-symmetry directions in the *bcc* Brillouin zone and the real part of $E(\mathbf{k})$ was analyzed. Experimental lattice and atomic coordinates determined from both x-ray and neutron diffraction studies were used in these computations.[30,34] For final crystal potentials and atomic charges (converged below 1 m Ry and 10^{-4}e, respectively), total site-decomposed and *l*-decomposed densities of states were computed at few hundred energy points using the tetrahedron method for integration in the reciprocal space. The thermopower was roughly estimated from numerical derivation of the DOS near the Fermi level, E_F.

III. RESULTS AND DISCUSSION

A. Band-structure calculations

The total density of states at the Fermi level, $N(E_F)$, and the site-decomposed densities of states of the Mo, Ru, Sb1, and Sb2 atoms as a function of the energy are presented in Fig. 2. The compositional dependence of the partial densities of states have been previously discussed and revealed that the $x=0.50$ concentration delineates two regions.[30] Below this value, $N(E_F)$ is only slowly lowered by increasing the Ru content while for higher x values, a more pronounced decrease occurs. All contributions vanish for $x=1$ revealing a

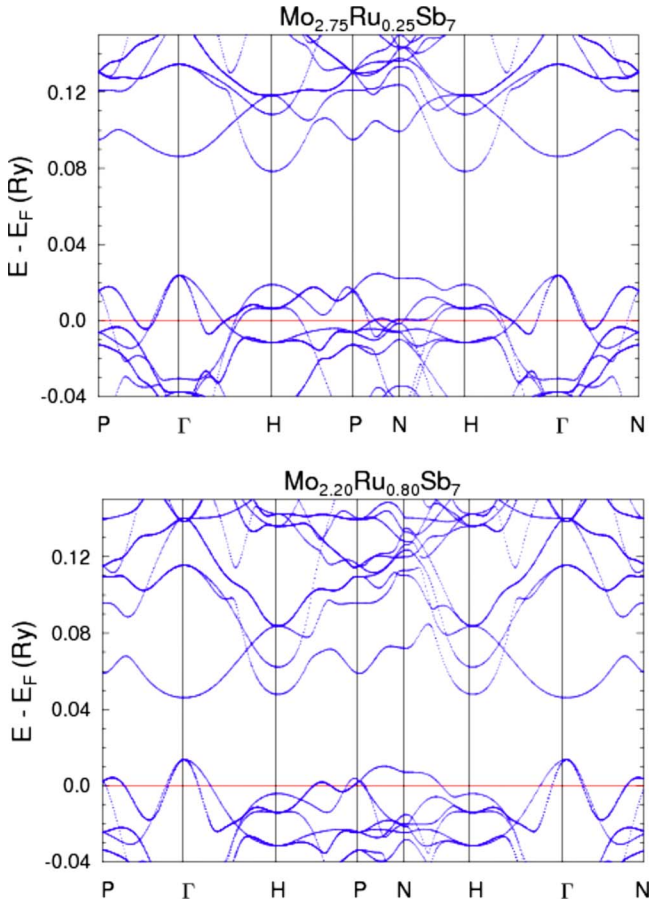

FIG. 3. (Color online) Dispersion curves along high-symmetry directions for the x=0.25 and 0.8 samples.

changeover from a metallic state to a semiconducting regime of conduction. Furthermore, whatever the Ru content, the main contributions to $N(E_F)$ come from the Mo and to a less extent from the Ru atoms. As Fig. 2 attests to, the energy dependence of $N(E)$ provides further theoretical evidence in favor of a rigidlike behavior of the electronic structure as the Ru content increases. The presence of ruthenium in the Mo_3Sb_7 crystalline lattice does not exert any strong influence on the shape of the valence bands in the vicinity of the Fermi level. This behavior can be also clearly distinguished on the dispersion curves calculated for the x=0.25 and 0.8 samples (Fig. 3). With increasing x, one can notice a slight decrease in the energy gap (appearing between the Γ and H points) as well as a relative lowering of the band energy occurring near the H point. However, both the degeneracy and the curvature of the valence bands only slightly change along the $Mo_{3-x}Ru_xSb_7$ series of compounds supporting a rigidlike scenario.

Even though an accurate theoretical analysis of the thermopower would require integration in the reciprocal space and, therefore, complete information on k-dependent electron velocities and lifetime near the Fermi surface, an estimation of the linear term of the thermopower, α/T, can provide preliminary information on its variation with the Ru content using the Mott formula which is expressed as

$$\frac{\alpha}{T} = -\frac{\pi^2}{3}\frac{k_B^2}{e}\left.\frac{\partial \ln \sigma(E)}{\partial E}\right|_{E_F}, \quad (1)$$

where k_B is the Boltzmann constant, e is the elementary charge, and σ is the electrical conductivity. Assuming that σ is mainly driven by $N(E_F)$ and that the hole mobility is energy independent, α/T, extrapolated to T=0 K, can be then calculated. The obtained values are listed in Table II. As expected from the rigidlike behavior of the electronic structure, the thermopower should increase with increasing the ruthenium concentration.

B. Magnetic properties

The temperature dependence of the magnetic susceptibility, carefully extracted from the slope of the linear magnetization curves above 1 T (a small temperature-independent ferromagnetic contribution that saturates at low fields is present) is shown in Fig. 4. As we can see, the partial substitution of Mo by Ru drastically affects the low-dimensional magnetism exhibited by Mo_3Sb_7 and arising from antiferromagnetically coupled molybdenum dimers.[19] While the salient features that characterize the magnetic susceptibility of Mo_3Sb_7 (i.e., a maximum in the magnetic-susceptibility curve and a low-temperature dependence dominated by the spin gap below T^*) (Ref. 19) can still be observed for x =0.25 and recognizable for x=0.50, a very different picture emerges for x=0.80. At this concentration, the magnetic susceptibility displays negative values in the whole temperature range investigated, indicative of a diamagnetic behavior. Hence, the presence of ruthenium seems to result in the disappearance of the above-mentioned magnetic interactions as well as of the spin gap.[27] The partial substitution of Mo by Ru directly influences the molybdenum dimers since Ru atoms that carry a spin-1 act as impurities breaking the anti-

TABLE II. Total and partial DOS at E_F obtained from KKR-CPA calculations in the $Mo_{3-x}Ru_xSb_7$ compounds. Total and site-decomposed DOS at E_F as well as thermopower values evaluated at 50 and 100 K are expressed in states Ry^{-1}, $spin^{-1}$, and $f.u.^{-1}$, states Ry^{-1}, $spin^{-1}$, and $atom^{-1}$ and $\mu V\ K^{-1}$, respectively. The Stoner product $I_{Mo}N_{Mo}(E_F)$, where I_{Mo} is the exchange integral ($I_{Mo}\sim$0.027 Ry in the present case) and $N_{Mo}(E_F)$ is the partial DOS at the Fermi level of the Mo atoms, is also given.

Chemical formula	$N_{tot}(E_F)$	$N_{Mo}(E_F)$	$N_{Ru}(E_F)$	$N_{Sb1}(E_F)$	$N_{Sb2}(E_F)$	$I_{Mo}N_{Mo}(E_F)$	S_{50}	S_{100}
$Mo_{2.75}Ru_{0.25}Sb_7$	64.9	9.72	2.91	2.86	2.04	0.52	3.9	23.4
$Mo_{2.5}Ru_{0.5}Sb_7$	53.1	7.15	2.82	3.46	1.89	0.38	6.6	39.6
$Mo_{2.2}Ru_{0.8}Sb_7$	33.9	4.21	1.78	2.18	1.23	0.22	9.6	57.6

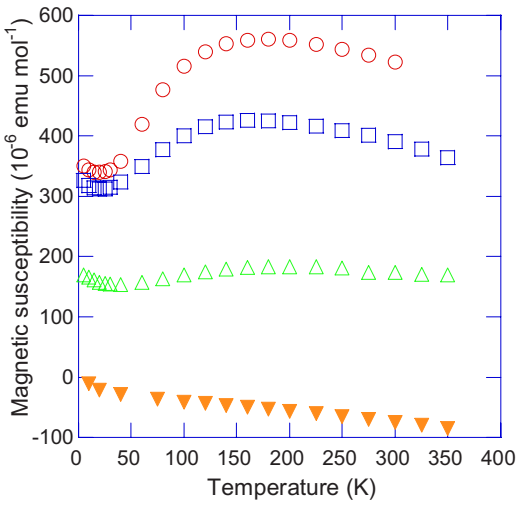

FIG. 4. (Color online) Temperature dependence of the molar magnetic susceptibility of the x=0 (○), 0.25 (□), 0.5 (△), and 0.8 (▼) samples.

ferromagnetic coupling between the spin-$\frac{1}{2}$ of the molybdenum atoms. Interestingly, the same behavior can be observed when the environment of the molybdenum dimers is modified, i.e., when Te substitutes Sb.[27] Neutron diffraction experiments performed on both systems have indicated that these substitutions lead to an increase in the Mo-Mo and Mo-Mo/Mo-Ru bond lengths in the $Mo_3Sb_{7-x}Te_x$ and $Mo_{3-x}Ru_xSb_7$ compounds, respectively, providing a possible crystallographic origin of the progressive suppression of these interactions. However, this increase is much less pronounced in the $Mo_3Sb_{7-x}Te_x$ compounds even for high Te concentrations and thus may indicate a more complex magnetic framework in Mo_3Sb_7. Koyama *et al.*[22] have suggested that both antiferromagnetic intradimer and interdimer interactions should be equally taken into account to explain the destabilization of the cubic state along only one crystallographic direction below T^* resulting in a possible magnetic frustration. Assuming that this picture is valid, the partial substitution of Mo by Ru may then affect the intradimer interactions while the partial substitution of Sb by Te may rather affect the interdimer interactions, both substitutions leading to the disappearance of the magnetic excitations and of the spin gap formation as well as of the structural deformation. In addition, the magnetic-susceptibility variations with x are consistent with a progressive crossover from a paramagnetic metal to a diamagnetic semiconductor as predicted by our KKR-CPA calculations.

Magnetic susceptibility data can provide a valuable insight into the variation in $N(E_F)$ with x as well as interesting information on the effective mass of the charge carriers. The density of states $N(E_F)$ of magnetically nonpolarized charge carriers is at the origin of the so-called Pauli susceptibility expressed via the free-electron formula[35]

$$\chi_{\text{Pauli}} = 2.376 \times 10^{-6} \times N(E_F). \tag{2}$$

In Eq. (2), χ_{Pauli} and $N(E_F)$ are expressed in emu mol^{-1} and in states Ry^{-1}, respectively. To extract the experimental Pauli temperature-independent contribution, the magnetic susceptibility, χ_0, for all studied samples can be written as

$$\chi_0 = \chi_{\text{Pauli}} + \chi_{core} + \chi_{CW}, \tag{3}$$

where χ_{CW} stands for the low-temperature Curie-Weiss tail of localized moments (likely related to paramagnetic impurities) and χ_{core} represents the temperature-independent core diamagnetism of the constituent species that can be estimated using Pascal's constants.[36] χ_{Pauli} values can be then evaluated by extrapolating the $\chi - \chi_{core}$ curves to 0 K. It is worthwhile to mention that because of the low-temperature Curie-Weiss tail clearly noticeable for the x=0.0, 0.25, and 0.50 samples we performed a fit to the data to subtract this contribution. Table III summarizes the theoretical and experimental $N(E_F)$ values along with the various obtained magnetic contributions. As can be observed, $N(E_F)$ decreases with x as suggested by our KKR-CPA calculations.

Besides the evolution of the electronic structure, the experimental Pauli susceptibility combined with the theoretical $N(E_F)$ values can be used to estimate the reduced effective mass of the charge carriers m^*/m_0 from Eq. (4) (Ref. 35)

$$\chi_{\text{Pauli}} = \left(\frac{m^*}{m_0} - \frac{1}{3}\frac{m_0}{m^*}\right)\chi_{\text{Pauli}}^{\text{KKR-CPA}}, \tag{4}$$

where m_0 stands for the free-electron mass of the noninteracting electrons. The high m^*/m_0 values (Table III) are similar to those inferred for the $Mo_3Sb_{7-x}Te_x$ compounds and show only small variations across the entire Ru concentration range.[27]

C. Transport and magnetotransport properties

The temperature dependence of the electrical resistivity of the $Mo_{3-x}Ru_xSb_7$ samples is reported in Fig. 5. The first essential feature lies in positive electrical resistivity coefficient $d\rho/dT$ for all samples indicative of a metal-like character.

TABLE III. Values of the theoretical $[N(E_F)_{\text{KKR-CPA}}]$ and experimental $[N(E_F)_{\text{Exp}}]$ densities of states at the Fermi level, diamagnetic contribution χ_{dia}, Pauli susceptibility inferred from experimental data (χ_{Pauli}) and band-structure calculations ($\chi_{Pauli}^{\text{KKR-CPA}}$) together with the derived values of the reduced effective masses m^*/m_0 using Eq. (3) for x=0, 0.25, 0.5, and 0.8.

Chemical formula	$N(E_F)_{\text{KKR-CPA}}$ (states Ry^{-1} f.u.$^{-1}$)	$\chi_{\text{Pauli}}^{\text{KKR-CPA}}$ (10^{-6} emu mol^{-1})	χ_{dia} (10^{-6} emu mol^{-1})	χ_{Pauli} (10^{-6} emu mol^{-1})	$N(E_F)_{\text{exp}}$ (states Ry^{-1} f.u.$^{-1}$)	m^*/m_0
Mo_3Sb_7	166	395	280	650	261	1.8
$Mo_{2.75}Ru_{0.25}Sb_7$	129	307	280	590	247	2.1
$Mo_{2.5}Ru_{0.5}Sb_7$	108	257	280	430	226	1.8
$Mo_{2.2}Ru_{0.8}Sb_7$	68	162	280	280	186	1.9

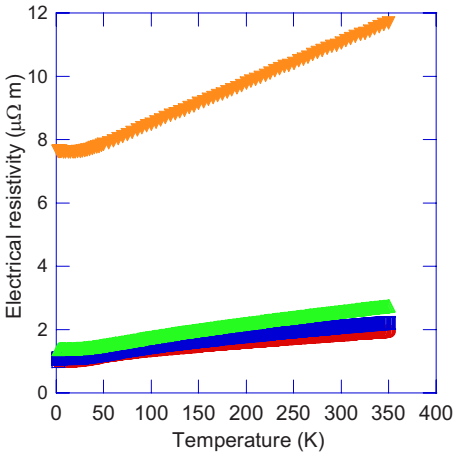

FIG. 5. (Color online) Temperature dependence of the electrical resistivity of the $x=0$ (○), 0.25 (□), 0.5 (△), and 0.8 (▼) samples.

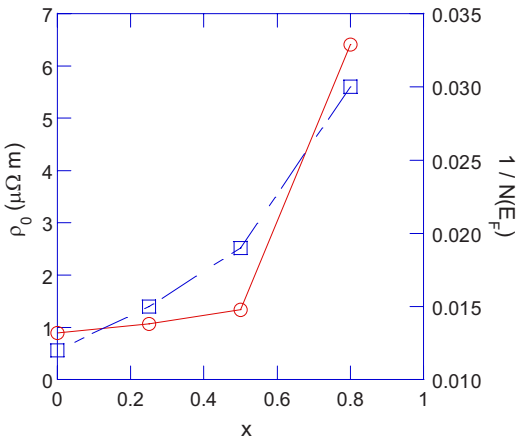

FIG. 6. (Color online) Residual electrical resistivity ρ_0 (○) and $1/N(E_F)$ (□) values as a function of the Ru content. Note that the ρ_0 values have been corrected to take into account the relative density of the samples.

Thus, because the Ru content is lower than the theoretical value ($x=1$) required to shift the Fermi level at the edge of the valence band, a semiconducting state is not yet reached at these concentrations, which appears consistent with our band-structure calculations. The exotic behavior exhibited by the electrical resistivity of Mo_3Sb_7 has been ascribed to the spin gap formation leading to downward curvature near T^* and below this temperature, a dependence that can be modeled by a thermal activation law.[19] Ruthenium insertion on the molybdenum site affects these characteristics. While the $x=0.25$ and 0.50 samples display similar variations, the electrical resistivity decreases, exhibits a minimum and then slowly increases when the temperature increases for $x=0.80$. The disappearance of the aforementioned features further corroborates the magnetic susceptibility data revealing the suppression of the magnetic interactions at high Ru concentration. As x is increased, the magnitude of ρ slightly increases for $0.0<x\leq 0.50$ and shows a pronounced jump for $x=0.80$. The lower relative density of the latter sample (Table II) only partially accounts for the observed behavior. As revealed by our KKR-CPA calculations, a rapid decrease in $N(E_F)$ occurs for $x\geq 0.50$.[30] Therefore, the higher electrical resistivity values displayed by the $x=0.80$ sample seem to show that the electrical resistivity of the $Mo_{3-x}Ru_xSb_7$ system is mainly driven by $N(E_F)$, as expected from a rigid-like behavior of the electronic structure. This viewpoint is further supported by the residual electrical resistivity, ρ_0, and $1/N(E_F)$ values that follow a similar variation as a function of the Ru content (Fig. 6).

Further evidence for this picture is provided by the magnetotransport data. Whatever the Ru concentration is, all samples display a positive Hall coefficient, R_H, in the whole temperature range investigated, indicative of hole conduction. As already underlined in the case of the Mo_3Sb_7 and $Mo_3Sb_{7-x}Te_x$ compounds,[26,27] the Hall resistivity, ρ_H, shows strong variations with magnetic field at low temperature for samples that still exhibit magnetic interactions, i.e., for $x=0.0$, 0.25, and 0.50. Since such low-dimensional magnetism makes the separation of the anomalous contribution from the measured data a complex task, information on the carrier concentration could only be obtained at room temperature (RT) for the $x=0.25$ and 0.50 samples. At the maximum Ru content that could be achieved, magnetic interactions can no longer be distinguished and concomitantly the superlinear magnetic-field dependence of ρ_H is strongly lessened. Restoring the linearity in $\rho_H=f(B)$ with increasing x is consistent with Hall-effect measurements performed in the $Mo_3Sb_{7-x}Te_x$ system and among all, raises the question whether or not a superlinear magnetic-field dependence can be considered as a common feature of spin gap compounds. Further experimental investigations on other materials displaying magnetically coupled dimers would be very revealing in substantiating this hypothesis.

Nevertheless, useful information regarding the hole concentration and their mobilities can be inferred from room-temperature magnetotransport data. Assuming the presence of only one type of carriers and a parabolic dispersion rela-

TABLE IV. Hole concentration (p), Hall mobility (μ_H), Seebeck coefficient (α), electrical resistivity (ρ), and thermal conductivity (λ) measured at RT for the different $Mo_{3-x}Ru_xSb_7$ compounds studied.

Chemical formula	p (cm^{-3})	μ_H ($cm^2\ V^{-1}\ s^{-1}$)	α ($\mu V\ K^{-1}$)	ρ ($\mu\Omega$ m)	λ ($W\ m^{-1}\ K^{-1}$)
Mo_3Sb_7	8.5×10^{21}	4.1	18	1.8	6.2
$Mo_{2.75}Ru_{0.25}Sb_7$	6.0×10^{21}	5.0	19	2.1	4.9
$Mo_{2.5}Ru_{0.5}Sb_7$	2.4×10^{21}	10.0	33	2.5	5.2
$Mo_{2.2}Ru_{0.8}Sb_7$	1.2×10^{21}	5.0	62	11.2	3.8

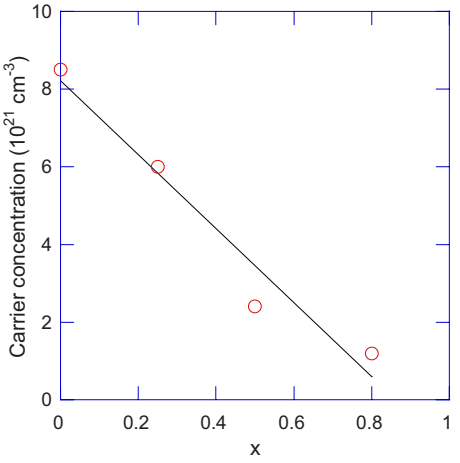

FIG. 7. (Color online) Carrier concentration as a function of the Ru content.

tion, the hole concentration, p, can be estimated from the simple relation $p=1/R_H e$ (Table IV). As shown in Fig. 7, p decreases quasilinearly as the Ru content increases. This dependence demonstrates that p can be adjusted without significantly altering the electronic band structure and stands for a strong evidence that variations in the electrical properties of these materials can be understood within a rigid-band model. In addition, the $x=0.80$ sample exhibits a temperature-independent behavior suggesting that the Fermi level is not yet positioned into the gap, in perfect agreement with the band-structure calculations (Fig. 8).

Using the room-temperature experimental values of both the electrical resistivity and Hall coefficient, the Hall mobility, $\mu_H=R_H/\rho$, can be calculated for all samples studied (Table IV). The low values obtained are consistent with the high carrier concentrations displayed by these compounds. In the case of the $x=0.80$ sample, the temperature dependence of μ_H is shown in the inset of Fig. 8. Below 100 K, the

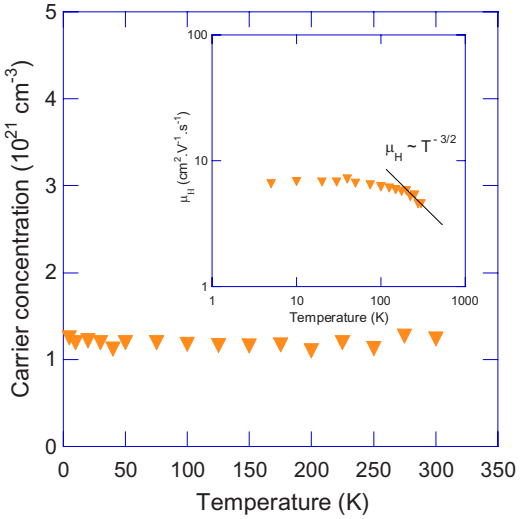

FIG. 8. (Color online) Temperature dependence of the hole concentration of the $x=0.8$ sample. Inset: Hall mobility as a function of the temperature for $x=0.8$. The solid line denotes the expected temperature dependence accounting for acoustic phonon scattering.

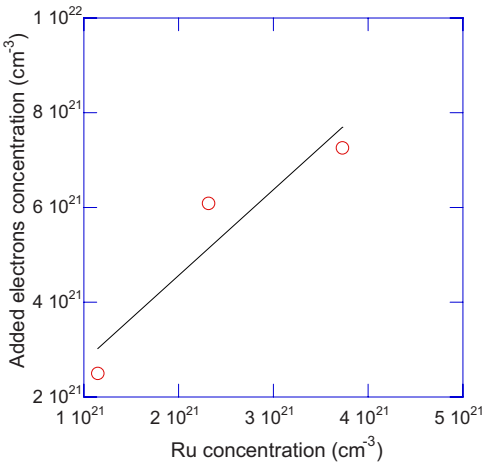

FIG. 9. (Color online) Electrons added to the structure as a function of the Ru concentration. The slope of the solid line leads to an estimation of the number of electrons given per Ru atom.

mobility is temperature-independent suggestive of scattering by neutral impurities. Above this temperature, μ_H decreases with temperature following roughly a $T^{-3/2}$ dependence near room temperature indicative of a charge-carriers scattering dominated by acoustic phonons.

One of the key questions that arises when Ru substitutes Mo lies in the number of electrons delivered by the Ru atoms to the Mo_3Sb_7 structure. Theoretical investigations have shown that two electrons should be given by Ru atoms to drive the system into a semiconducting state. If the solubility limit of Ru which is lower than the required value can naturally explain the absence of conduction crossover, this characteristic could be coupled with a different number of electrons added per Ru atom preventing to reach a semiconducting state even for a hypothetical $x=1.0$ concentration. This last hypothesis can be experimentally investigated by considering the electron concentration added to the structure as a function of the Ru concentration (Fig. 9). The electron concentration added increases roughly linearly with x. The slope of the line then leads to an estimation of the

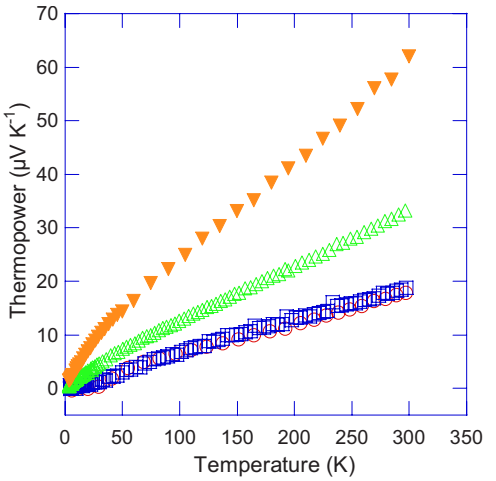

FIG. 10. (Color online) Temperature dependence of the thermopower for the $x=0$ (○), 0.25 (□), 0.5 (△), and 0.8 (▼) samples.

TABLE V. Effective masses (m^*/m_0), reduced Fermi level (η), and Lorenz number (L) estimated from Eqs. (5) and (6) and Eq. (11) of Ref. 27, respectively.

Chemical formula	m^*/m_0	η	L (10^{-8} V^2 K^{-2})
$Mo_{2.75}Ru_{0.25}Sb_7$	3.1	14.9	2.40
$Mo_{2.5}Ru_{0.5}Sb_7$	2.9	8.6	2.33
$Mo_{2.2}Ru_{0.8}Sb_7$	3.4	4.5	2.14

electrons added per Ru atoms. In the present case, it amounts to 1.8 electrons per Ru atoms, a value very close to that expected based on electron configuration and rigid-band picture. Thus, it seems that the solubility limit of ruthenium in the Mo_3Sb_7 structure can mainly be held responsible for the absence of semiconducting behavior in these compounds.

The temperature dependence of the thermopower is illustrated in Fig. 10. For all samples, α is positive in the whole temperature range indicative of an electrical conduction dominated by holes, in perfect agreement with the Hall-effect data. As can be observed, an increase in the Ru content leads to an increase in the magnitude of α, consistent with a progressive decrease in the hole concentration. In addition to the diffusive contribution to the thermopower, an additional contribution typified by a slight curvature at low temperature is revealed for all samples. A similar feature is displayed by the $Mo_3Sb_{7-x}Te_x$ compounds and has been tentatively ascribed to a phonon-drag contribution.[27] Likewise, this effect could manifest itself in the isostructural $Mo_{3-x}Ru_xSb_7$ compounds.

KKR-CPA calculations have provided theoretical insights into the effective mass of the charge carriers and the position of the Fermi level as x increases. Both properties can be experimentally explored by numerically estimating the hole effective masses and by considering the degree of degeneracy displayed by these materials, respectively. The former property can be investigated at room temperature within a single parabolic band model and using the experimental values of the thermopower and hole concentration. The temperature dependence of the Hall mobility has suggested that acoustic phonons stand for the main source of charge-carrier diffusion near room temperature in the $x=0.80$ compound. The thermopower and hole concentration are then expressed as[7]

$$\alpha = -\frac{k_B}{e}\left[\frac{2F_1(\eta)}{F_0(\eta)} - \eta\right], \tag{5}$$

$$p = \frac{4}{\sqrt{\pi}}\left(\frac{2\pi m^* k_B T}{h^2}\right)^{3/2} F_{1/2}(\eta), \tag{6}$$

where F_i is the Fermi integral of order i, η is the reduced Fermi level defined as $\eta = E_F/k_BT$, and h is the Planck constant. Assuming that this model can be extended to lower Ru concentration, the calculated values of the reduced effective masses m^*/m_0 and Fermi level η are summarized in Table V for all compounds studied. As can be observed, η decreases

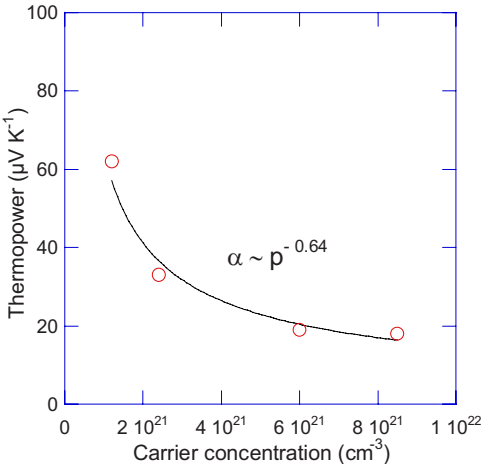

FIG. 11. (Color online) Thermopower as a function of the carrier concentration. The solid line represents the best fit to the data according to the relation [Eq. (7)].

when the Ru content increases consistent with a progressive crossover from a metallic to a semiconducting state. The relatively high value displayed by the $x=0.80$ sample together with quasiconstant effective masses across the entire Ru concentration range suggest that all samples can still be considered as highly degenerate. Thus, Fermi-Dirac statistics are no longer required and Fermi integrals can be simplified. Equations (5) and (6) can then be replaced by Eq. (7) indicating that the thermopower should linearly increase with temperature and should exhibit a $p^{-2/3}$ dependence[37]

$$\alpha = \frac{8\pi^2 k_B^2}{3eh^2} m^* T\left(\frac{\pi}{3p}\right)^{2/3}. \tag{7}$$

As shown in Fig. 11, the experimental thermopower values of the $Mo_{3-x}Ru_xSb_7$ compounds follow this last trend. A fit of the data with the exponent as a free parameter reveals an excellent agreement between the experimental and theoretical variations.

The temperature dependence of the total thermal conductivity for all samples studied is presented in Fig. 12(a). To compare the thermal conductivity of these compounds from each other, all the data have been corrected using the model developed by Landauer to take into account the difference in the relative densities of the samples (see Table I).[38] The exotic behavior exhibited by the Mo_3Sb_7 compound has been ascribed to an interplay between phonons and magnetic interactions, the latter constituting the main scattering source of the former. In addition, the minimum observed near 50 K has been attributed to the formation of the spin gap. As already observed in the $Mo_3Sb_{7-x}Te_x$ series, the total thermal conductivity increases with x below ~150 K.[27] Above 200 K, a usual behavior is almost recovered, i.e., a decrease in the total thermal conductivity with increasing the Ru content [the $x=0.25$ and 0.50 samples do not follow this trend but at higher temperature (350–1000 K) a conventional behavior against the Ru content is observed, see Ref. 31].

The absence of a minimum in the thermal conductivity of the $x=0.25$ sample constitutes another evidence of a close

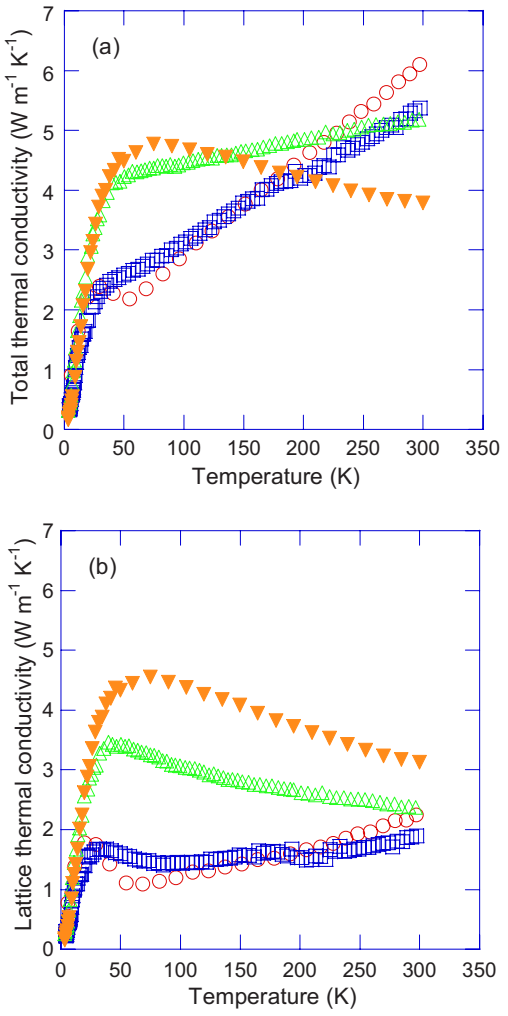

FIG. 12. (Color online) (a) Total thermal conductivity as a function of the temperature for the $x=0$ (○), 0.25 (□), 0.5 (△), and 0.8 (▼) samples. (b) Lattice thermal conductivity of the four compounds investigated.

relationship between the exotic magnetism and the minimum in thermal conductivity near 50 K exhibited by the binary compound. This puzzling behavior shows that the thermal conductivity increases with increasing the unit-cell disorder while the opposite trend is usually observed and desired, at least from a thermoelectric point of view. Since the electrical resistivity of these samples increases with x, this behavior seems to be conditioned by an increase in the lattice thermal conductivity. To separate the lattice contribution, λ_l, from the total thermal conductivity, we subtracted the electronic contribution, λ_e, using the Wiedemann-Franz law

$$\lambda_e = \frac{LT}{\rho}, \tag{8}$$

where T is the absolute temperature and L the Lorenz number. The analysis of the effective masses of these compounds has revealed that the Ru-substituted samples can still be considered as highly degenerate. Thus, we can guess that fixing L to the value of a degenerate electron gas, i.e., $L=L_0=2.44\times10^{-8}$ V^2 K^{-2} should constitute a reasonable approximation. Nonetheless, assuming that acoustic phonons scattering is the prominent scattering mechanism at play in these materials, as suggested by the temperature dependence of the Hall mobility, the actual Lorenz number can then be estimated (Table V).[27] As expected, such determined Lorenz numbers are very close to L_0.

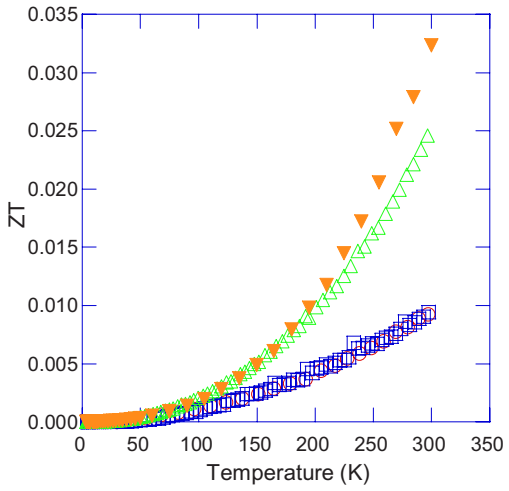

FIG. 13. (Color online) Temperature dependence of the thermoelectric figure of merit for the $x=0$ (○), 0.25 (□), 0.5 (△), and 0.8 (▼) samples.

However, since the mechanisms governing the transport properties of the $Mo_3Sb_{7-x}Te_x$ and $Mo_{3-x}Ru_xSb_7$ compounds are similar, we can anticipate that the magnetic interactions should have a marked impact on L, resulting in deviations of L from L_0 at low temperatures. High-temperature thermoelectric properties measurements performed on both family seem to further corroborate this picture.[29,31] Assuming $L=L_0$ would then lead to an electronic contribution that could surpass the total thermal conductivity at high temperature, indicating that additional scattering mechanisms most likely related to the magnetic interactions might exist.[26,31] Consequently, as the estimation of the actual Lorenz number, which takes into account the effect of the magnetic interactions, cannot be simply undertaken within current theories, we have estimated the lattice thermal conductivity illustrated in Fig. 12(b) as a function of the temperature by assuming $L=L_0$. It is worth mentioning that considering lower L values would modify neither the observed trend nor our analysis.

In the case of the $Mo_3Sb_{7-x}Te_x$ compounds, the concomitant increase in the thermal conductivity with the disappearance of the magnetic interactions has been held responsible for the observed and unexpected behavior.[27] Since similar properties are displayed by the $Mo_{3-x}Ru_xSb_7$ compounds, the Ru content dependence of λ_l also strongly suggests an intimate interplay between phonons and antiferromagnetically coupled dimers.

Based on the measured thermoelectric properties, the temperature dependence of the thermoelectric figure of merit, ZT, can be calculated and is plotted in Fig. 13 for the four samples studied. The ZT values increase with increasing temperature and as expected with Ru concentration. The values obtained for the $x=0.50$ and 0.80 samples (0.025 and 0.033 at 300 K, respectively) are higher than those reported in the

$Mo_3Sb_{7-x}Te_x$ compounds (~0.02 at 300 K for $x=1.6$).[27]

IV. SUMMARY

Transport and magnetic-susceptibility measurements coupled with KKR-CPA band-structure calculations have been performed on a series of polycrystalline samples of $Mo_{3-x}Ru_xSb_7$ for $x=0.0$, 0.25, 0.50, and 0.80. The partial substitution of Mo by Ru has a deep impact on the magnetic interactions exhibited by Mo_3Sb_7 as demonstrated by the magnetic-susceptibility data. One of the unforeseen consequences of the disappearance of these interactions lies in the increase in the total thermal conductivity with x. Even though the solubility limit of Ru prevents to reach a semiconducting state, both thermopower and electrical resistivity values increase with x, consistent with our KKR-CPA calculations predicting a rigidlike behavior of the electronic structure.

ACKNOWLEDGMENTS

C.C. greatly thanks M. Amiet and P. Maigné, and the financial support of DGA (Délégation Générale pour l'Armement, Ministry of Defense, France) and the European Network of Excellence CMA (Complex Metallic Alloys). J.T. acknowledges the support of the Polish Ministry of Science and Higher Education (Grants No. N202-2104-33 and No. 44/N-COST/2007/0). C. Bellouard is warmly thanked for her assistance in galvanomagnetic and magnetic experiments.

*Corresponding author. Present address: Max-Planck-Institut für Chemische Physik fester Stoffe, Nöthnitzer Str. 40, 01187 Dresden, Germany; christophe.candolfi@mines.inpl-nancy.fr; candolfi@cpfs.mpg.de

[1] S. M. Kauzlarich, S. R. Brown, and G. J. Snyder, Dalton Trans. **2007**, 2099.
[2] F. Gascoin, S. Ottensmann, D. Stark, S. M. Haile, and G. J. Snyder, Adv. Funct. Mater. **15**, 1860 (2005).
[3] X.-J. Wang, M.-B. Tang, J.-T. Zhao, H.-H. Chen, and X.-X. Yang, Appl. Phys. Lett. **90**, 232107 (2007).
[4] C. Yu, T. J. Zhu, S. N. Zhang, X. B. Zhao, J. He, Z. Su, and T. M. Tritt, J. Appl. Phys. **104**, 013705 (2008).
[5] X.-J. Wang, M.-B. Tang, H.-H. Chen, X.-X. Yang, J.-T. Zhao, U. Burkhardt, and Yu. Grin, Appl. Phys. Lett. **94**, 092106 (2009).
[6] H. Zhang, J.-T. Zhao, Yu. Grin, X.-J. Wang, M.-B. Tang, Z.-Y. Man, H.-H. Chen, and X.-X. Yang, J. Chem. Phys. **129**, 164713 (2008) and references therein.
[7] H. J. Goldsmid, *Thermoelectric Refrigeration* (Temple Press Ltd., London, 1964).
[8] S. R. Brown, S. M. Kauzlarich, F. Gascoin, and G. J. Snyder, Chem. Mater. **18**, 1873 (2006).
[9] S. R. Brown, E. S. Toberer, T. Ikeda, C. A. Cox, F. Gascoin, S. M. Kauzlarich, and G. J. Snyder, Chem. Mater. **20**, 3412 (2008).
[10] E. S. Toberer, C. A. Cox, S. R. Brown, T. Ikeda, A. F. May, S. M. Kauzlarich, and G. J. Snyder, Adv. Funct. Mater. **18**, 2795 (2008).
[11] E. S. Toberer, S. R. Brown, T. Ikeda, S. M. Kauzlarich, and G. J. Snyder, Appl. Phys. Lett. **93**, 062110 (2008).
[12] U. Häussermann, M. Elding-Ponten, C. Svensson, and S. Lidin, Chem.-Eur. J. **4**, 1007 (1998).
[13] A. Brown, Nature (London) **206**, 502 (1965).
[14] E. Dashjav, A. Szczepenowska, and H. Kleinke, J. Mater. Chem. **12**, 345 (2002).
[15] F. Gascoin, J. Rasmussen, and G. J. Snyder, J. Alloys Compd. **427**, 324 (2007).
[16] N. Soheilnia, H. Xu, H. Zhang, T. M. Tritt, I. Swainson, and H. Kleinke, Chem. Mater. **19**, 4063 (2007).
[17] C. Candolfi, B. Lenoir, A. Dauscher, C. Bellouard, J. Hejtmanek, E. Santava, and J. Tobola, Phys. Rev. Lett. **99**, 037006 (2007).
[18] C. Candolfi, B. Lenoir, A. Dauscher, J. Hejtmanek, E. Santava, and J. Tobola, Phys. Rev. B **77**, 092509 (2008).
[19] V. H. Tran, W. Miiller, and Z. Bukowski, Phys. Rev. Lett. **100**, 137004 (2008).
[20] Z. Bukowski, D. Badurski, J. Stepien-Damm, and R. Troc, Solid State Commun. **123**, 283 (2002).
[21] R. Khasanov, P. W. Klamut, A. Shengelaya, Z. Bukowski, I. M. Savic, C. Baines, and H. Keller, Phys. Rev. B **78**, 014502 (2008).
[22] T. Koyama, H. Yamashita, Y. Takahashi, T. Kohara, I. Watanabe, Y. Tabata, and H. Nakamura, Phys. Rev. Lett. **101**, 126404 (2008).
[23] A. B. Karki, D. P. Young, P. W. Adams, E. K. Okudzeto, and Julia. Y. Chan, Phys. Rev. B **77**, 212503 (2008).
[24] B. Wiendlocha, J. Tobola, M. Sternik, S. Kaprzyk, K. Parlinski and A. M. Oles, Phys. Rev. B **78**, 060507(R) (2008).
[25] T. Koyama, H. Yamashita, T. Kohara, Y. Tabata, and H. Nakamura, Mater. Res. Bull. **44**, 1132 (2009).
[26] C. Candolfi, B. Lenoir, A. Dauscher, E. Guilmeau, J. Hejtmanek, J. Tobola, B. Wiendlocha, and S. Kaprzyk, Phys. Rev. B **79**, 035114 (2009).
[27] C. Candolfi, B. Lenoir, A. Dauscher, J. Hejtmanek, and J. Tobola, Phys. Rev. B **79**, 235108 (2009).
[28] C. Candolfi, B. Lenoir, A. Dauscher, J. Tobola, S. J. Clarke, and R. I. Smith, Chem. Mater. **20**, 6556 (2008).
[29] C. Candolfi, B. Lenoir, C. Chubilleau, A. Dauscher and E. Guilmeau, (unpublished).
[30] C. Candolfi, B. Lenoir, J. Leszczynski, A. Dauscher, J. Tobola, S. J. Clarke, and R. I. Smith, Inorg. Chem. **48**, 5216 (2009).
[31] C. Candolfi, B. Lenoir, J. Leszczsynki, A. Dauscher, and E. Guilmeau, J. Appl. Phys. **105**, 083701 (2009).
[32] J. Korringa, Physica **13**, 392 (1947); W. Kohn and N. Rostoker, Phys. Rev. **94**, 1111 (1954).
[33] A. Bansil, S. Kaprzyk, P. E. Mijnarends, and J. Tobola, Phys. Rev. B **60**, 13396 (1999).
[34] Neutron-diffraction experiments did not reveal any ordering of the Ru atoms on the Mo site. Hence, Ru atoms were considered to randomly occupy the Mo sublattice.
[35] S. V. Vonsovskii, *Magnetism* (Wiley, New York, 1974), Vol. 1.
[36] L. N. Mulay and E. A. Boudreaux, *Theory and Applications of Molecular Diamagnetism* (Wiley, New York, 1976).
[37] M. Cutler, J. F. Leavy, and R. L. Fitzpatrick, Phys. Rev. **133**, A1143 (1964).
[38] R. Landauer, J. Appl. Phys. **23**, 779 (1952).